JOURNAL OF GUIDANCE, CONTROL, AND DYNAMICS
Vol. 17, No. 5, September–October 1994

Robust Identification and Vibration Suppression of a Flexible Structure

John L. Crassidis*
Goddard Space Flight Center, Greenbelt, Maryland 20771
Donald J. Leo† and Daniel J. Inman‡
Virginia Polytechnic Institute and State University, Blacksburg, Virginia 24061
and
D. Joseph Mook§
State University of New York at Buffalo, Buffalo, New York 14260

A robust vibration suppression design involving the use of H_∞ optimal control theory is studied for a complex flexible structure. The digital control architecture involves noncollocated feedback utilizing active piezoceramic actuators and position sensor data. The modal properties of the multi-input, multi-output structure are first determined from experimental data in order to obtain an identified state-space model. This model forms the basis for the H_∞ vibration suppression design. Performance specifications are developed that obtain adequate damping in the structure while maintaining controller integrity without the destabilization of higher modes. A controller optimized for these H_∞ performance specifications is implemented on the actual test structure. Experimental structural perturbations are also examined in order to determine the robustness of the vibration suppression design. The experimental study indicates that the H_∞ design substantially increases damping in the targeted frequency region and conforms to predicted analytical simulations.

Introduction

SPACE structures are generally very flexible and have many degrees of freedom in both the bending and torsional modes. The problem of controlling these structures has been investigated vigorously in the past,[1–3] by utilizing both active and passive damping control techniques. Previous work has demonstrated the potential of using active strut elements to improve the vibrational response of a structure.[4] The application of these active elements to a noncollocated structural control problem can enhance system performance while tailoring the input-output properties of the structure.

The H_∞ control strategy, as compared to classical control techniques, provides new techniques and perspectives in designing control systems. This is accomplished by shaping the frequency response characteristics of a plant according to prespecified performance specifications in the form of weighting functions. The H_∞ design process is chosen since 1) it supplies robust stability to model and sensor uncertainties, 2) it achieves performance requirements efficiently, 3) it handles both disturbance and controller saturation problems easily, and 4) it works not only on simple single-input, single-output (SISO) systems but also on multi-input, multi-output (MIMO) systems.[5] Therefore, frequency response criteria can easily be shaped to desired specifications.

In recent years the implementation of robust stabilization and control based on H_∞ control theory has been investigated for different structures.[6,7] However, most of these studies are limited to analytical simulations. A common procedure first involves the generation of a finite element model for the structure. Collocated rate feedback is often implemented in order to damp certain modes and to facilitate a reduced-order model used in the H_∞ design process. However, experimental implementation of collocated velocity feedback can lead to stability problems if a priori precautions of actuator dynamics are not taken.[8,9] In particular, the control of low-frequency modes could destabilize the intermediate and higher modes. Also, the closed-loop response characteristics are sensitive to the plant model used in the H_∞ design. If significant error exists between the nominal model and the actual system, then experimental results could drastically differ from analytical simulations.

Recent experimental verification of applying an H_∞ design for active vibration suppression has shown more practical solutions to this control problem. Fanson et al.[2] have demonstrated that a noncollocated robust control approach can provide satisfactory performance characteristics in structures with and without passive damping. However, differences exist between experimental results and theoretical responses, due to significant error between the nominal (finite element) model and the actual structure. Stroughton and Voth[10] have shown that a collocated robust control design for a highly damped structure could be developed. This design is insensitive to fairly large errors in specific structural modes. However, the controller is of high order, which imposes extensive computational burden. The intent of this paper is to develop a low-order H_∞ controller that provides structural damping in a flexible structure using noncollocated sensors and actuators. Noncollocated control of a flexible structure is difficult to achieve since low damping and non-minimum-phase characteristics are inherent in the system.

In recent years, several time-domain techniques have become useful for structural testing.[11–13] In most circumstances, time-domain identification algorithms have advantages over conventional frequency-domain algorithms, including higher testing speed, better resolution of modes in high-modal-density bandwidths, and lower cost of instrumentation.[14] Therefore, time-domain techniques for flexible-structure realization and identification are useful in determining state-space models, which are required for the H_∞ control design. In most circumstances, the identification of SISO models from experimental data can easily be obtained. However, since transmission zeros impose strict mathematical constraints on system matrices, minimal realizations of MIMO systems are usually difficult to obtain experimentally. Possible sources of error include sensor and instrumentation noise, slight nonlinearities inherent in the structure, and/or background vibration. Therefore, for system identification of flexible structures, multiple experiments are usually performed in

Received Dec. 24, 1992; revision received Oct. 4, 1993; accepted for publication Jan. 20, 1994.

*NRC Resident Research Associate, Guidance and Control Branch. Member AIAA.
†Research Assistant, Department of Engineering Science and Mechanics. Associate Fellow AIAA.
‡Samuel Herrick Professor, Department of Engineering Science and Mechanics. Associate Fellow AIAA.
§Associate Professor, Department of Mechanical and Aerospace Engineering. Senior Member AIAA.

order to improve mathematical models. However, this requires extensive computational time and effort.

The identification algorithm used in this paper identifies accurate (near-minimal) realizations of a structure from only one set of experimental data. This algorithm combines an optimal state estimation routine, known as the minimum model error (MME) estimator,[15,16] with the eigensystem realization algorithm[17] (ERA) in order to provide robust features for MIMO identification. In several previous studies, this algorithm has been successfully applied to numerous applications, including nonlinear estimation[18] and robust realization/identification of mode shapes in damped structures.[19–20]

The μ-synthesis approach[21] utilizes robust performance techniques in order to alleviate deviations in the nominal model. However, this methodology usually results in high-order controllers if the nominal model has a large number of uncertainties. Also, the choice of uncertainty weights requires some level of iteration and intuition in order to achieve the required performance characteristics. The design procedure in this paper involves the determination of an accurately identified model from experimental data, so that the use of uncertainty weighting can be minimized.

Robustness, with respect to parameter and structural changes, is an important aspect to any control design. The use of multiplicative and additive uncertainty singular-value relationships can help determine which modes are sensitive to structural variations.[5] Of particular interest is the suppression (damping) of lower modes without the destabilization of high-frequency modes. The aid of accurate model representations, using the MME/ERA identification algorithm, can lead to a clearer coherence between experimental results and theoretical predictions. Therefore, model and structural uncertainties can be studied in order to test the robustness and sensitivity of the H_∞ controller on the closed-loop system.

The organization of this paper proceeds as follows. First, a brief overview of the H_∞ control theory and design methodology is presented. Then, the experimental implementation and system hardware for the structure are shown. The identified model is then realized into state-space form by using the combined MME/ERA identification algorithm. This model is incorporated with H_∞ performance specifications for vibration suppression and controller frequency-response shaping. Two designs are presented. One design stresses active damping in the first two modes of the structure, and the other design stresses robust stability over a higher system bandwidth. Each of these control designs are experimentally implemented and results are compared to theoretical computer simulations.

H_∞ Overview

This section gives a brief overview of the fundamental theory of H_∞ control design. The H_∞ norm of a transfer function matrix represents the maximum energy in the output signal from the transfer function due to any input of unit energy. Therefore, minimizing the H_∞ norm of a transfer function is equivalent to minimizing the energy in the output signal due to the inputs.[5]

In order to demonstrate the fundamental aspects of H_∞ control theory, consider a system with controller $F(s)$ and plant $G(s)$. The sensitivity function $(I + FG)^{-1}$ is defined as the transfer function from the output disturbance $D(s)$ to the plant output $Y(s)$. Then, if a stabilizing controller F is chosen such that $\|(I + FG)^{-1}\|_\infty$ is minimized, the energy of the plant output due to a disturbance of bounded energy is minimized. Similarly, the output controller function $F(I + FG)^{-1}$ is the transfer function from the reference input $R(s)$ to the controller output $U(s)$. Minimizing $\|F(I + FG)^{-1}\|_\infty$ constrains controller output energy and also maximizes allowable additive plant uncertainty.[5] Finally, the complementary sensitivity function $FG(I + FG)^{-1}$ is the transfer function from the reference input to the plant output. Minimizing $\|FG(I + FG)^{-1}\|_\infty$ tailors plant output energy to input reference commands. The H_∞ design process considers these closed-loop performances to prespecified weighting functions, denoted as $\gamma W_1(j\omega)$, $W_2(j\omega)$, and $W_3(j\omega)$. The H_∞ optimization problem is to find a stabilizing controller $F(s)$ that minimizes

$$\left\| \begin{matrix} \gamma W_1(I + FG)^{-1} \\ W_2F(I + FG)^{-1} \\ W_3FG(I + FG)^{-1} \end{matrix} \right\|_\infty \tag{1}$$

Equation (1) also shapes the frequency loop transfer function $L(s) = G(s)F(s)$ by penalizing the sensitivity function to reject plant disturbances, and the high-frequency $L(s)$ by penalizing the complementary sensitivity to cope with model uncertainties, while maintaining controller output to desired specifications. The solution of the H_∞ control problem involves an iteration on the γ term of the specified disturbance weighting function. As γ is increased, the sensitivity function $S(s)$ decreases, whereas the complementary sensitivity function $(I - S)$ approaches the W_3^{-1} weighting function.

H_∞ Design with Active Damping

The mixed-sensitivity approach[22] in Eq. (1) shows a clear tradeoff between performance and robustness of a multivariable system. However, this methodology does not enable a practical design approach for active damping, since plant dynamics are usually canceled with compensator dynamics. This section expands upon the fundamental H_∞ control formulation in order to provide a means of incorporating active damping into a structure with inherently low structural damping ratios (well below 0.50% critical).

Consider the block diagram of a MIMO plant in Fig. 1. Let the MIMO plant $[G(s)]$ be partitioned into "disturbance" $[G_1(s)]$ and "plant/actuator" $[G_2(s)]$ transfer functions, i.e.,

$$Y_2(s) = G_1(s)U_{1a}(s) + G_2(s)U_2(s) \tag{2}$$

The partitioned transfer functions have ideally the same characteristic polynomial and differ only in numerator dynamics. The inputs in Fig. 1 are $U_{1a}(s)$, any disturbance input into the structure (noncollocated with the actuator), and $U_{1b}(s)$, a fictitious input used to simulate the sensor uncertainty. The "augmented" plant with control compensator is shown in Fig. 2.

The open-loop transfer function matrix of the augmented plant is

$$\begin{bmatrix} y_{1a} \\ y_{1b} \\ y_{1c} \\ -- \\ y_2 \end{bmatrix} = \left[\begin{array}{cc|c} W_1G_1 & W_1 & -W_1G_2 \\ 0 & 0 & W_2 \\ 0 & 0 & W_3G_2 \\ -- & -- & -- \\ G_1 & I & -G_2 \end{array}\right] \begin{bmatrix} u_{1a} \\ u_{1b} \\ -- \\ u_2 \end{bmatrix} \tag{3}$$

where u_2 and y_2 are controller output and input, respectively. The sensitivity function between the disturbance input and the plant output now becomes

$$\frac{e}{u_{1a}} = \frac{G_1}{I + FG_2} \tag{4}$$

Therefore, active damping can be accomplished, since pole locations of the closed-loop transfer function in Eq. (4) are shifted by

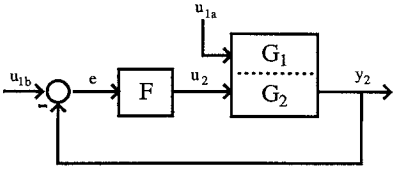

Fig. 1 Multi-input, multi-output block diagram.

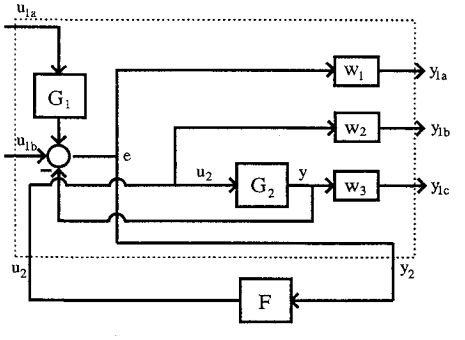

Fig. 2 Augmented closed-loop system.

the controller (F) and plant/actuator transfer functions. From Fig. 2, the characteristics of the weighting function $W_1(s)$ determines the amount of damping and frequency-response dynamics of the closed-loop systems. The complementary sensitivity (sensor uncertainty) function and controller/limiter function remain unchanged from the previous section. Also, once the augmented plant in Eq. (3) is formed, numerical algorithms for the computation of the optimal controller can be utilized. This controller solution is determined by the two-Riccati algorithm[23] using the Robust Control Toolbox[24] for MATLAB.

Experimental Hardware

A clamped frame serves as a testbed for the experimental H_∞ control implementation. The structure consists of 39 elements connected at 18 nodes. All but two of the structural members are made from thin-walled circular aluminum tubing with an outer diameter of 0.25 in. and a wall thickness of 0.05 in. Each member is pinned and bolted into the nodes to eliminate looseness in the joints. The frame is configured in a planar fashion so that the only significant deformation occurs perpendicular to the structure (see Fig. 3).

Two of the structural members are flat aluminium bars layered with piezoceramics. Either of these struts can excite the frame since a voltage applied across the piezoceramics produces a moment on the frame. The strut on the bottom of the frame has four ceramics glued to it and serves as the control actuator. The other flat strut is configured with the same number of piezoceramics and acts as a disturbance source. Each of these active members has a thickness of 0.25 in. and a width of 1.0625 in. The piezoceramics are model G-1195 from Piezo Electric Products, with dimensions 2.5 × 0.75 ×0.01 in.

The sensor is a Philtec (model 88NE3) optical displacement sensor placed near node 18 at the free end of the frame. This sensor is noncollocated with both the control actuator and the disturbance source. Frequency analysis and data acquisition are performed using a Tektronix 2630 Fourier analyzer. Control laws are implemented on an Optima 3 digital controller, sampling at a rate of 500 Hz. This sampling rate allows the maximum allowable performance for the H_∞ controller design. Finally, two Hewlett Packard amplifiers (model 6924A) are used to magnify the control and disturbance signals. A more detailed description of the experimental hardware and setup can be found in Ref. 25.

Robust System Estimation and Identification

An accurate state-space model of the testbed is required in order to perform an optimal control design. In this work, the ERA[17] is combined with the MME[15] optimal estimator in order to update a finite element (nominal) model to conform with experimental data. The finite element model provides a fairly accurate representation of the frame at the lower modes, as shown in Figs. 4 and 5. However, the higher modes are not modeled accurately. This could cause the destabilization of higher modes when implementing the controller onto the actual structure.

The ERA method is effective for developing accurate state-space models when noise levels are low in nature. However, difficulties arise when higher noise levels are present in the output measurements. These effects can make a minimal state-space model of a MIMO system extremely difficult to obtain, since transmission zeros

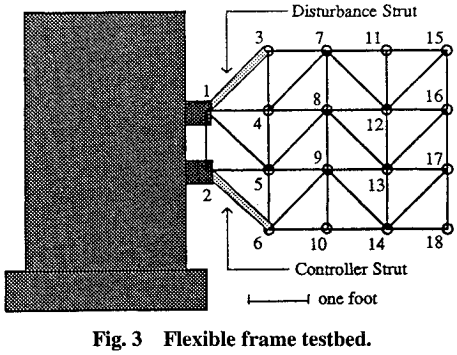

Fig. 3 Flexible frame testbed.

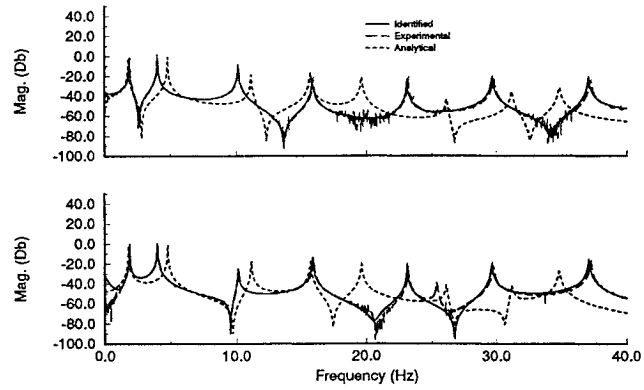

Fig. 4 Experimental, analytical, and identified magnitude plots (first input).

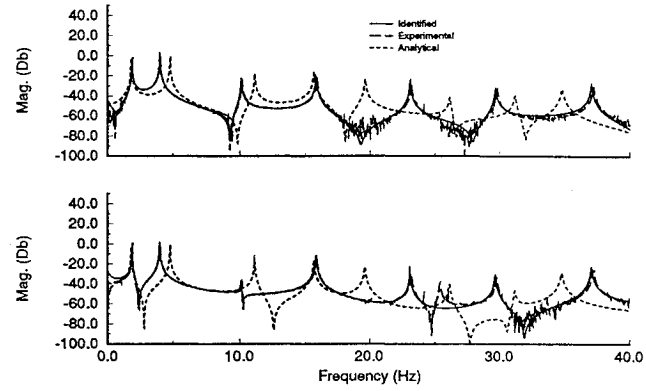

Fig. 5 Experimental, analytical, and identified magnitude plots (second input).

also constrain the realization. For the identification of the testbed the ERA is able to identify the natural frequencies and damping ratios fairly accurately using an average of three different time histories. But a near-minimal MIMO realization of the testbed could not be obtained. By combining the ERA with the MME estimator, which utilizes the minimal state-space MIMO finite element model, improved modal identification is achieved with near-minimal MIMO realizations.

In this section, the MME algorithm is briefly reviewed for the case of linear, time-variant state-space models. A more detailed derivation of the algorithm may be found in Ref. 15. The MME algorithm assumes that the state estimates are given by a nominal (prespecified) model and an unmodeled error vector, shown as

$$\begin{aligned} \dot{\hat{\boldsymbol{x}}}(t) &= A_m(t)\hat{\boldsymbol{x}}(t) + B_m(t)u(t) + \boldsymbol{d}(t) \\ \hat{\boldsymbol{y}}(t) &= C_m(t)\hat{\boldsymbol{x}}(t) + D_m(t)u(t) \end{aligned} \tag{5}$$

where $A_m(t)$, $B_m(t)$, $C_m(t)$, and $D_m(t)$ are time-variant nominal state matrices from the finite element model, $u(t)$ is a $p \times 1$ known forcing input, $\boldsymbol{d}(t)$ is an $n \times 1$ unmodeled (to-be-determined) model error vector, $\hat{\boldsymbol{x}}(t)$ is the $n \times 1$ state estimate vector, and $\hat{\boldsymbol{y}}(t)$ is the $q \times 1$ estimated output. For the remainder of this paper, the state-space (model) matrices are assumed time variant but are shown without the time argument (t).

State-observable discrete time-domain measurements are assumed for Eq. (5) in the following form:

$$\tilde{\boldsymbol{y}}(t_k) = \boldsymbol{g}_k(\boldsymbol{x}(t_k),\ t_k) + \nu_k \tag{6}$$

where $\tilde{\boldsymbol{y}}(t_k)$ is an $q \times 1$ measurement vector at time t_k, $\boldsymbol{g}_k$ is an accurate model of the measurement process, ν_k represents measurement noise, and m is the total number of measurement output sets. The measurement noise process is assumed to be a zero-mean, Gaussian distributed process of known covariance R.

In the MME, the optimal state estimates are determined on the basis that the measurement-minus-estimate error covariance matrix

must match the measurement-minus-truth error covariance matrix. This condition is referred to as the covariance constraint, approximated by

$$\left\{[\tilde{y}(t_k) - \hat{y}(t_k)][\tilde{y}(t_k) - \hat{y}(t_k)]^T\right\} \approx R \tag{7}$$

Therefore, the estimated measurements are required to fit the actual measurements with approximately the same error covariance as the actual measurements fit the truth.

A cost functional, consisting of the weighted sum square of the measurement-minus-estimate residuals plus the weighted sum square of the model correction term, is next minimized:

$$J = \sum_{k=1}^{m} \left\{[\tilde{y}(t_k) - \hat{y}(t_k)]^T R^{-1} [\tilde{y}(t_k) - \hat{y}(t_k)]\right\} + \int_{t_0}^{t_f} \mathbf{d}(\tau)^T W\, \mathbf{d}(\tau)\, \mathbf{d}\tau \tag{8}$$

where W is a weight matrix determined by satisfying the covariance constraint. If the measurement residual covariance is larger than R, then the measurement estimate is not close to the actual system measurements. Therefore, W should be decreased in order to more penalize the model correction $[d(t)]$. However, if the estimate covariance is too low, then W should be increased in order to allow less model correction. The model error corrects the finite element model in order to estimate the output using experimental measurements. Therefore, the model error term tends to update the finite element model to conform to actual system responses.

The necessary conditions for the minimization of J, with respect to the model correction term $d(t)$ leads to the following two-point boundary-value problem (TPBVP)[15]:

$$\begin{aligned} \dot{\hat{\boldsymbol{x}}}(t) &= A_m \hat{\boldsymbol{x}}(t) + B_m \boldsymbol{u}(t) + \mathbf{d}(t) \\ \dot{\boldsymbol{\lambda}}(t) &= -A_m^T \boldsymbol{\lambda}(t) \\ \boldsymbol{d}(t) &= -\tfrac{1}{2} W^{-1} \boldsymbol{\lambda}(t) \\ \boldsymbol{\lambda}(t_k^+) &= \boldsymbol{\lambda}(t_k^-) + 2C_m^T R^{-1} [\tilde{\boldsymbol{y}}(t_k) - \hat{\boldsymbol{y}}(t_k)] \end{aligned} \tag{9}$$

where $\lambda(t)$ is a vector of costates (Lagrange multipliers). Also, the costate equation is updated at each measurement interval. The boundary conditions are selected such that either $\boldsymbol{\lambda}(t_0^-) = \mathbf{0}$ or $\boldsymbol{x}(t_0)$ is specified for the initial time and either $\boldsymbol{\lambda}(t_f^+) = \mathbf{0}$ or $\boldsymbol{x}(t_f)$is specified at the final time. The solution of the TPBVP involves the determination of a linear Riccati equation and a linear differential equation.[16]

Modified Eigensystem Realization Algorithm

The ERA method is a modal synthesis technique based on the concept of singular-value decomposition (see Ref. 17 for more details). This procedure is capable of accurately identifying the model properties of systems involving perfect or low-noise measurements. In this section the ERA is expanded to include the state and output estimates given by the MME estimator.

Consider the discrete-time linear dynamic equation

$$\begin{aligned} \boldsymbol{x}(k+1) &= A\boldsymbol{x}(k) + B\boldsymbol{u}(k) \\ y(k) &= C\boldsymbol{x}(k) + D\boldsymbol{u}(k) \end{aligned} \tag{10}$$

where $\boldsymbol{x}$ is a $n \times 1$ state vector, $\boldsymbol{u}$ is a $p \times 1$ input vector, y is a $q \times 1$ output vector; A, B, and C are $n \times n$, $n \times p$, and $q \times n$ constant matrices, respectively. A solution to Eq. (10) is given by the Markov parameters from a unit impulse response:

$$Y(k) = CA^{k-1}B \qquad X(k) = A^{k-1}B \tag{11}$$

The first step in the modified ERA is to form an $r \times s$ block Hankel matrix composed of the impulse response data from the MME algorithm:

$$H(k-1) = \begin{bmatrix} Z(k) & \cdots & Z(k+m_s-1) \\ \vdots & \ddots & \vdots \\ Z(k+l_{r-1}) & \cdots & Z(k+l_{r-1}+m_{s-1}) \end{bmatrix} \tag{12}$$

where r and s are arbitrary integers satisfying the inequalities $rq \geq n$ and $sp \geq n$ and l_i $(i = 1, 2, \ldots, r-1)$ and m_j $(j = 1, 2, \ldots, s-1)$ are arbitrary integers. The vector Z consists of the estimated output and states given by the MME estimator, i.e., $z = [\hat{x} \quad \hat{y}]^T$. The singular-value decomposition of H may be expressed as $H = PD_nQ$. The ERA then forms the discrete-time, reduced-order model realization of dimension n in the following form:

$$\begin{aligned} A &= D_n^{-1/2} P_n^T H(1) Q_n D_n^{-1/2} \\ B &= D_n^{1/2} Q_n^T E_p \\ C &= E_q^T P_n D_n^{1/2} \\ D &= Y(0) \end{aligned} \tag{13}$$

where P_n and Q_n are formed from the first n columns of P and Q from the singular-value decomposition and D_n is the diagonal matrix of singular values. Here E_p^T is $[I_p, 0]$ and E_q^T is $[I_q, 0]$, where I_p and I_q are identity matrices of order p and q, respectively, and 0 is the zero matrix.

The modal damping ratios and damped natural frequencies are calculated by observing the real and imaginary parts of the eigenvalues after a transformation from the z plane to the s plane is completed.[17] The physical mode shapes of the system are determined using the realized eigenvectors (Φ) of the ERA state matrices. The physical mode shapes are given by $\Psi = C_m\Phi$. Physical state matrices can be determined by using this mode shape matrix and the continuous eigenvalue matrix:

$$A_m = \Psi[\Lambda]\Psi^{-1}$$

$$B_m = \Psi \begin{bmatrix} e^{\lambda_1 \Delta t}/\lambda_1 & 0 & \cdots & 0 \\ 0 & \ddots & & 0 \\ \vdots & & \ddots & \vdots \\ 0 & 0 & \cdots & e^{\lambda_n \Delta t}/\lambda_n \end{bmatrix}^{-1} \Psi^{-1} B \tag{14}$$

where Λ is the continuous eigenvalue matrix, derived from a discrete to continuous eigenvalue transformation of the ERA state matrix. Therefore, an identification of system parameters is possible by using the physical state matrices shown in Eq. (14).

Combined Realization Algorithm

The combined MME/ERA algorithm enables the realization of a MIMO model in the presence of significant model error, process noise, and measurement noise. In order to obtain impulse response data, the test structure is excited using a random input with a bandwidth of 0–50 Hz. An inverse and regular Fourier transformation is applied on these data to obtain the impulse-response time histories. Also, only one set of data for each input is taken for the identification. Therefore, extensive and repetitive computational analysis is attenuated by using the combined MME/ERA method, since averaging of multiple sets of data is not needed. This is an important aspect due to the difficulty of obtaining multiple sets of experimental data for orbiting space structures.

A block diagram illustrating the steps of the robust realization algorithm is shown in Fig. 6. First, the finite element model is used as the assumed model in the MME estimator. Next, the MME estimation problem is solved, using the covariance constraint to determine an optimal weighting matrix. The continuous estimated state histories produced from the MME are then resampled. Finally, these estimated time histories are processed, in order to realize an accurate model of the system parameters, using the modified version of the ERA. These steps may be repeated if necessary in order to further

Table 1 Poles of the identified model

Mode	ω, Hz	ζ, %
1	1.91	0.46
2	4.00	0.25
3	10.14	0.21
4	15.80	0.20
5	23.10	0.13
6	29.67	0.17
7	37.06	0.13
8	48.36	0.45
9	49.00	0.36
10	54.55	0.25
11	56.08	0.27
Lights	60.00	0.00
Real	0.20	

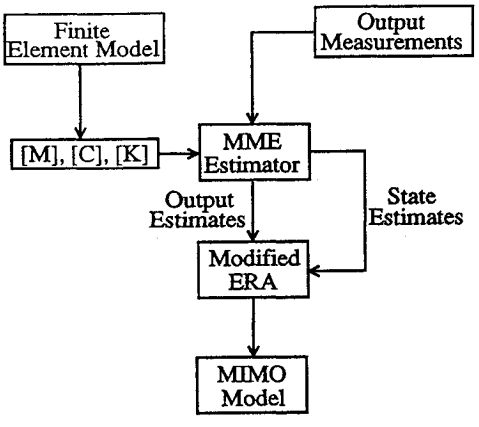

Fig. 6 Block diagram of combined realization algorithm.

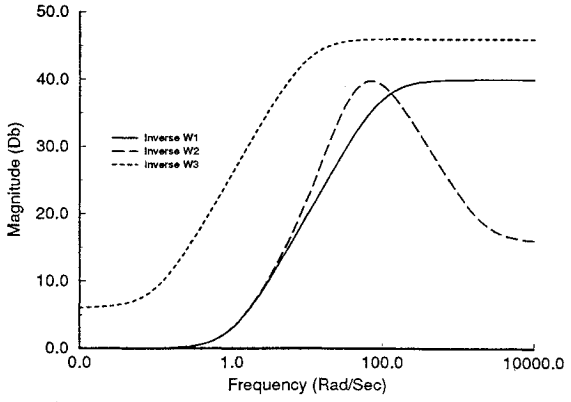

Fig. 7 Magnitude plots of inverse weighting functions.

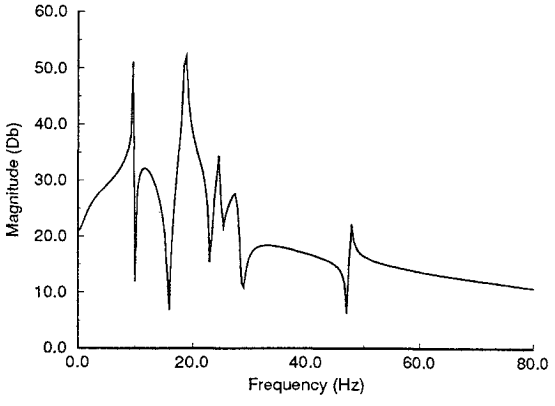

Fig. 8 Magnitude plot of robust controller.

smooth the measurements and improve the identification process. However, accurate identification results for this testbed required only one iteration through the MME estimation process.

The model properties for the first 11 flexible modes of the frame are shown in Table 1. The frame has all of the characteristics of a large flexible structure. It is modally dense, with 11 modes in the first 60 Hz bandwidth. Also, inherent damping in the structure is low, with modes having damping ratios less than 0.50%. The combined algorithm also identifies the frequency-response characteristics of the in-room fluorescent lighting at about 60 Hz.

Magnitude Bode plots of the MME/ERA identification results are compared to experimental frequency-response characteristics in Figs. 4 and 5 (also shown is the finite element model frequency plot). The MME/ERA produced a near minimal realization (24th order) for the first 11 modes. This MIMO model is extremely accurate with good agreement to experimental frequency-response results. Also, the modal amplitude coherence[17] (MAC) factors are substantially improved when using the combined MME/ERA algorithm. Therefore, this MIMO state-space model forms the basis for the robust control design.

Robust Control Design

In this section the concepts and limitations for the selection of the proper weighting functions used in the H_∞ design are presented. The appropriate selection of weighting functions over the desired frequency range is not explicitly related to the performance objectives in a straightforward manner. Numerous trial selections are usually required in order to obtain desired performance objectives. The goal of the H_∞ design is to reshape the open-loop dynamics in order to provide vibration suppression in the frequency region considered. Therefore, the sensitivity function in Eq. (4) is utilized to reshape these desired frequency characteristics and provide adequate damping to the structure. The complementary sensitivity function is used as an uncertainty weight for the sensor output. After careful consideration and numerous trials, a set of proper inverse weighting functions is obtained. The inverse weighting functions for the sensitivity and complementary sensitivity functions are shown in Fig. 7. The W_1^{-1} function weights the sensitivity function along the zero decibel region over a desired frequency. Damping can be added to the system by decreasing the overall magnitude of this weighting function (accomplished by increasing γ in the control solution formulation). The W_3^{-1} frequency function invokes a higher weight at lower frequencies with a first-order roll-off at higher frequencies. This limits the low-frequency noise from the sensor so that it is not amplified through the controller.

The inverse weighting function for the controller output is also shown in Fig. 7. The desired characteristic of the controller is to obtain an attenuated controller response at lower *and* higher frequencies. This results in a third-order weighting function that simulates a band-pass filter. The choice of this weighting function ensures that the controller does not destabilize higher frequency modes and also attenuates control signals at lower frequencies.

The selection of these weighting functions provides adequate damping in the closed-loop system. An optimal H_∞ controller solution using the γ iteration technique is determined with these weighting functions. The controller is found to be proper and rational. Since the augmented state-space model, derived from Eq. (3), is 29th order, the subsequent H_∞ controller is also 29th order. The Schur balanced model reduction method[24] is used to reduce this controller. The size of the resulting controller is 15th order. The frequency-response characteristic of the control design is shown in Fig. 8. The controller size is the maximum allowable order for the digital computer implementation. The next section summarizes the closed-loop results and shows a comparison between analytical simulations and experimental results.

Experimental Control Results

In this section, the H_∞ controller is experimentally implemented onto the testbed in order to test the validity of the identification and control techniques previously described. Results show that the performance objectives can be met with a significant increase in damping for more than one mode. Model uncertainties are also experimentally investigated, and the results are compared to theoretical predictions.

Table 2 System results for two controller designs and perturbations

		System		Nominal		First perturbation		Second perturbation	
	Mode number	ω_n	ζ, %	ω_n	ζ, %	ω_n	ζ, %	ω_n	ζ, %
Initial controller	1	1.91	0.46	1.95	6.32	1.95	6.55	Unstable	
	2	4.00	0.25	4.41	7.51	4.44	6.57	Unstable	
Second controller	1	1.91	0.46	1.91	1.94	1.91	1.93	1.59	1.56
	2	4.00	0.25	4.12	2.56	4.11	2.50	3.93	2.62

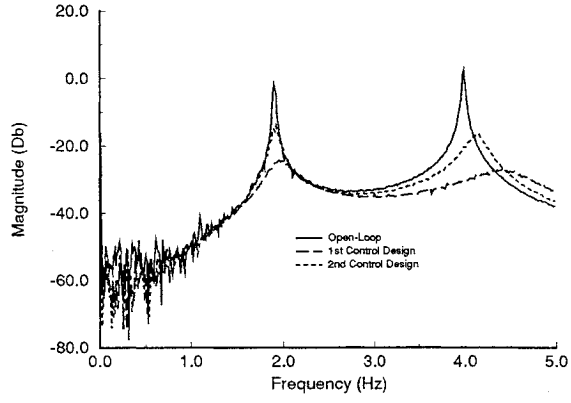

Fig. 9 Closed-loop and open-loop transfer function magnitude plots.

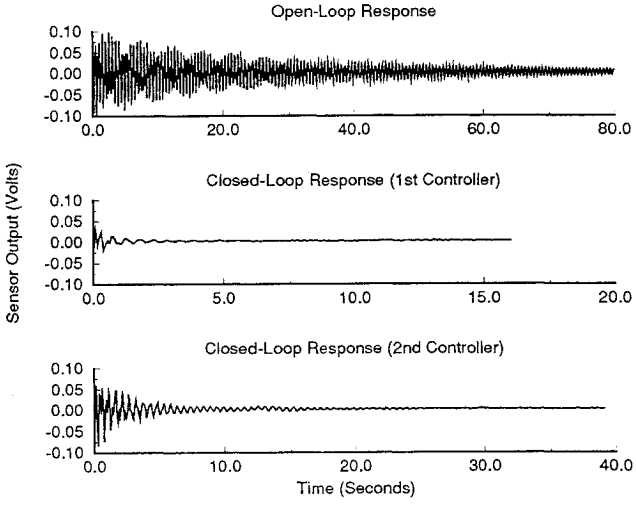

Fig. 10 Closed-loop and open-loop time responses.

The initial H_∞ controller design (shown in Fig. 8) is found to substantially increase the damping in the first two modes without the destabilization of higher modes. Digital implementation of this controller onto the testbed increases the damping in the first mode (bending) by a factor of about 14 ($\zeta_{cl} = 6.32\%$) and the second mode (torsional) by a factor of about 30 ($\zeta_{cl} = 7.51\%$). These results are summarized in Table 2 (the table also gives results for perturbed systems and a second control design, each described later). Slight damping is also provided in higher frequency modes. The closed-loop transfer function between the disturbance input and position sensor for the first two modes is shown in Fig. 9. The H_∞ controller is able to significantly provide active damping in the targeted frequency region. Figure 10 shows the position sensor output to a random noise input (bandwidth of 0–5 Hz) applied at the disturbance strut. Both open-loop and closed-loop responses are shown. Without the H_∞ controller, the vibration of the frame does not settle out for well over 80 s. Not only does closing the loop attenuate the level of vibration by over 75%, but also the increase in damping reduces the settling time to less that 4 s. In fact, the closed-loop response has a magnitude near the noise level of the sensor.

With the nominal design complete, model and structural uncertainties are next studied in order to test the robustness and sensitivity

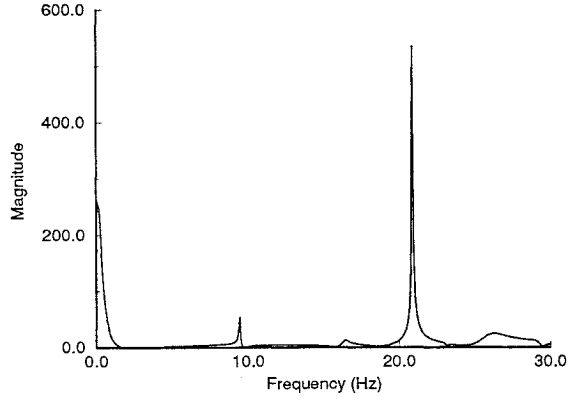

Fig. 11 Theoretical multiplicative uncertainty bound.

of the H_∞ controller on the closed-loop system. This is accomplished by varying the modal properties of the frame while utilizing the controller designed for the nominal system. The net effect on the structure is to incorporate multiplicative perturbations into the system. The H_∞ norm of a system can be used to measure the stability margins of the nominal control design in the face of these perturbations. Applying small gain theory[5] to this uncertainty case, a sufficiency test for stability robustness with a multiplicative uncertainty input is given as

$$\bar{\sigma}[\Delta_m(s)] < \frac{1}{\bar{\sigma}\{F(s)[I + G(s)F(s)]\}^{-1}} \tag{15}$$

where $\Delta_m(s)$ denotes multiplicative uncertainties and $\bar{\sigma}$ denotes the maximum singular value over the desired frequency region. Therefore, a multiplicative uncertainty bound over all frequencies can be used to determine which frequency is most sensitive to multiplicative perturbations. A plot of the theoretical uncertainty bound for the initial control design using the nominal plant is shown in Fig. 11. From this figure, the frequency that is most sensitive to plant perturbations is the 23-Hz mode. Therefore, this mode is most likely to become unstable in the face of perturbations on the frame.

Multiplicative perturbations are accomplished experimentally by varying the modal properties of the frame while utilizing the initial (nominal) control design. The natural frequencies and mode shapes are altered by placing weights at various points along the frame. These weights have a mass of approximately 3–5% of the mass of the total structure. The first perturbation is to place the weights on nodes 4 and 5 on the testbed (see Fig. 3). The second perturbation is to place the weights on nodes 16 and 17 on the testbed. The resulting changes in natural frequencies for these perturbations are shown in Table 3. The first perturbation has an average deviation of about 10% from the nominal natural frequencies. The second perturbation has an average deviation of about 15%. The most significant changes occurs at higher frequencies. Therefore, the nominal H_∞ controller can be tested for stability and performance using the experimentally perturbed systems. The controller is first used with the weights on nodes 4 and 5. Results for the closed-loop damping ratios are shown in Table 2. Even with an average of 10% change from the nominal system, robust stability *and* performance are achieved, with almost equal damping ratios as the nominal system. The closed-loop results for the second perturbation show that the system becomes unstable. However, as theory predicts from the multiplicative uncertainty plot

Table 3 Natural frequencies ω (Hz) of perturbed models

Mode number	Nominal	First perturbation	Second perturbation
1	1.91	1.88	1.59
2	4.00	4.00	3.88
3	10.14	9.78	9.41
4	15.80	15.28	15.03
5	23.10	22.66	21.38
6	29.67	25.09	24.03
7	37.06	29.03	27.97
8	48.36	32.12	35.47
9	49.00	44.25	39.72
10	54.55	47.25	46.16

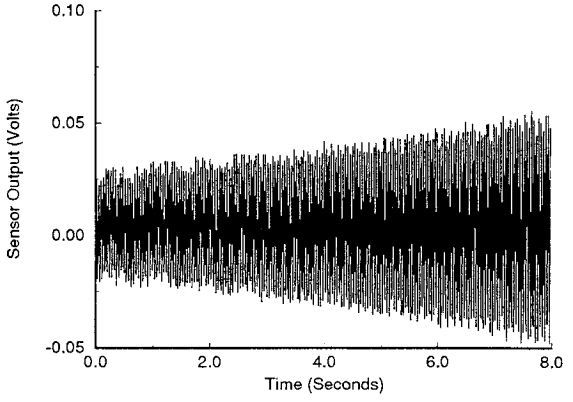

Fig. 12 Experimental instability using first perturbed system.

(Fig. 11), the closed-loop system becomes unstable at a frequency of about 23 Hz (shown in Fig. 12). Therefore, with the aid of accurate system models, the sensitivity of the H_∞ controller can be investigated and adjusted in order to compensate for perturbations *without* implementing the controller to the actual frame.

The second controller design provides more robust stability but decreases performance slightly. This controller is derived by simply decreasing the γ term during the H_∞ solution. The experimental closed-loop results for the nominal, first-perturbation, and second-perturbation systems are shown in Table 2. The magnitude frequency responses and time responses to a random input are also shown in Figs. 9 and 10, respectively. The nominal design increases damping by a factor of about 4 in the first mode and by a factor of about 10 in the second mode. This damping is less than the first controller design; however, the multiplicative uncertainty bound allows a greater perturbation at 23 Hz, as opposed to the initial controller design. Closed-loop results indicate that robust stability *and* performance are maintained for both perturbation systems (see Table 2). The second-perturbation system remains stable and has approximately the same increase in damping as the first-perturbation and nominal design, using the second controller.

The control of the frame is next tested by placing the sensor at various nodes along the frame. The sensor is next mounted at node 15 and the H_∞ control design is repeated. Results indicate that significant damping is again achieved in the first two modes with good agreement between theory and experiment. The control design for all cases involved SISO control of one node. The final control design is a MIMO controller with sensors placed at nodes 15 and 18. Theoretical results indicate that no significant increase in damping is achieved for the MIMO design. This is most likely due to the frame being controlled only by one strut. If multiple controller actuators are used, then greater possibilities of MIMO control can be achieved. The MME/ERA identification algorithm, is extremely useful for designing MIMO feedback loops, since accurate (near-minimal) realizations of MIMO systems are possible. Therefore, the extension to more complicated flexible frames can easily be accomplished using H_∞ control.

Finally, the increase in system performance is achieved without the use of any supplementary (low-authority) control. In many circumstances, passive damping elements and collocated control loops are first implemented in the design. The H_∞ controller is then used to further improve stability and performance. The results in this paper illustrate that system performance can be significantly improved and maintained in the face of modest perturbations without the use of supplementary control. Therefore, eliminating the need for supplementary active or passive damping decreases the complexity of the overall control problem.

Conclusions

A controller using H_∞ optimal control theory was designed and experimentally implemented to provide vibration suppression on a flexible frame structure. Time-domain data were first used to obtain an accurate MIMO model. The identification algorithm combined the MME estimator with the ERA in order to update a finite element model to conform with experimental data. Eleven flexible modes were found to be inside the frequency range of 0–60 Hz, all with damping ratios of less then 0.5% critical. This MIMO model formed the basis for the H_∞ control design.

A formulation designed to add active damping to the structure was determined for the control design. The closed-loop response characteristic of the structure was shaped by careful choice of three weighting functions. The first weight constrained sensor noise uncertainty. The second weight was designed to roll off the controller at low and high frequencies. The last weight controlled the amount of active damping in the structure. Experimental implementation of the H_∞ controller on the flexible frame validated the control formulation. Two control designs were considered. The first design provided significant damping in the first two modes but was sensitive to structural perturbations. The second design provided damping to a lesser degree, but supplied robust stability over significant perturbations to the structure. Results also indicate that with accurate model representations, the H_∞ controller can provide not only robust stability but also robust performance to modest system perturbations.

The difficult problem of designing a noncollocated controller for a flexible structure was handled well using H_∞ control theory. The framework in which the controller was designed was greatly simplified due to the accuracy of the identified state-space model. Reducing the complexity of the problem allowed a physical basis for choosing weighting functions. Therefore, the amount of effort needed to obtain and implement an H_∞ controller was greatly decreased.

References

[1]Cannon, R. H., and Rosenthal, D. E., "Experiments in Control of Flexible Structures with Noncollocated Sensors and Actuators," *Journal of Guidance, Control, and Dynamics*, Vol. 7, No. 5, 1984, pp. 546–553.

[2]Fanson, J. L., Lurie, B. J., O'Brien, J. F., Chu, C. C., and Smith, R. S., "System Identification and Control of the JPL Active Structure," *Proceedings of the 32nd Structures, Structural Dynamics, and Materials Conference* (Baltimore, MD), AIAA, Washington, DC, 1991, pp. 2237–2245.

[3]Wie, B., Horta, L., and Sulla, J., "Classical Control System Design and Experiment for the Mini-Mast Truss Structure," *Journal of Guidance, Control, and Dynamics*, Vol. 14, No. 4, 1991, pp. 778–784.

[4]Fanson, J. L., Chu, C. C., Smith, R. S., and Anderson, E. H., "Active Member Control of a Precision Truss Structure with an H_∞ Performance Objective," *Proceeding of the AIAA Dynamics Specialists Conference*, AIAA, Washington, DC, 1990, pp. 322–333.

[5]Tsen, F. M., "Optimal Design Techniques of H_∞ Control," Ph.D. Dissertation, State Univ. of New York at Buffalo, Buffalo, NY, Dec. 1991.

[6]Kashani, R., Melkote, S., and Sorgenfrei, A., "H_∞ Control of a Smart Structure Helicopter Rotor Blade," *Proceedings of the ASME Design Technical Conferences*, Miami, FL, 1991, pp. 27–31.

[7]Safonov, M. G., Chiang, R. Y., and Flashner, H., "H_∞ Robust Control Synthesis for a Large Space Structure," *Journal of Guidance, Control, and Dynamics*, Vol. 14, No. 3, 1991, pp. 513–519.

[8]Goh, C. J., and Caughey, T. K., "On the Stability Problem Caused by Finite Actuator Dynamics in the Collocated Control of Large Space Structures," *International Journal of Control*, Vol. 41, No. 3, 1985, pp. 787–802.

[9]Inman, D. J., "Control/Structure Interaction: Effects of Actuator Dynamics," *Mechanics and Control of Large Flexible Structures*, edited by J. L. Junkins, AIAA, Washington, DC, 1990, pp. 507–535.

[10]Stroughton, R. M., and Voth, C. T., "Vibration Suppression for a Large Space Structure Using H_∞ Control," *Proceedings of the AIAA Guidance, Navigation, and Control Conference*, AIAA, Washington, DC, 1991, pp. 458–466.

[11]Ibrahim, S. R., and Mikulcik, E. C., "A Method for the Direct Identification of Vibration Parameters from the Free Response," *Shock and Vibration Bulletin*, No. 47, Pt. 4, Sept. 1977, pp. 183–198.

[12]Yeh, F-B., and Yang, C-D., "New Time-Identification Technique," *Journal of Guidance, Control, and Dynamics*, Vol. 8, No. 4, 1987, pp. 463–470.

[13]Billings, S. A.,"Identification of Nonlinear Systems—A Survey," *Institute of Electrical and Electronic Engineers Proceedings*, Vol. 127, Pt. D, No. 6, 1980, pp. 272–285.

[14]Roemer, M., "Robust System Realization/Identification via Optimal State Estimation," Ph.D. Dissertation, State Univ. of New York at Buffalo, Buffalo, NY, 1991.

[15]Mook, D. J., and Junkins, J. L., "Minimum Model Error Estimation for Poorly Modeled Dynamic Systems," *Journal of Guidance, Control, and Dynamics*, Vol. 11, No. 3, 1988, pp. 256–261.

[16]Crassidis, J. L., Mason, P. A. C., and Mook, D. J., "A Riccati Solution for the Minimum Model Error Algorithm," *Journal of Guidance, Control, and Dynamics*, Vol. 16, No. 8, 1993, pp. 1181–1183.

[17]Juang, J-N., and Pappa, R. S., "An Eigensystem Realization Algorithm [ERA] for Modal Parameter Identification and Modal Reduction," *Journal of Guidance, Control, and Dynamics*, Vol. 8, No. 5, 1985, pp. 620–627.

[18]Stry, G. I., and Mook, D. J., "Experimental Study of Nonlinear Dynamics System Identification," *Nonlinear Dynamics*, Vol. 3, No. 1, 1992, pp. 1–11.

[19]Roemer, M. J., and Mook, D. J., "Robust Modal Identification/Estimation of the Mini-Mast Testbed," *Journal of Guidance, Control, and Dynamics*, Vol. 15, No. 3, 1992, pp. 642–647.

[20]Roemer, M. J., and Mook, D. J., "Enhanced Realization/Identification of Physical Modes," *ASCE Journal of Aerospace Engineering*, Vol. 3, No. 2, 1990, pp. 128–139.

[21]Balas, G. J., Packard, A. K., and Harduvel, J. T., "Application of μ-Synthesis Techniques to Momentum Management and Attitude Control of the Space Station," *Proceedings of the AIAA Guidance, Navigation, and Control Conference*, AIAA, Washington, DC, 1991, pp. 565–575.

[22]Francis, B. A., Helton, J. W., and Zames, G., "H_∞ Optimal Control for Linear Multivariate Systems," *Institute of Electrical and Electronic Engineers Transactions on Automatic Control*, Vol. AC-29, 1984, pp. 888–900.

[23]Doyle, J. C., Glover, K., Khargonekar, P. P., and Francis, B. A., "State-Space Solutions of Standard H_2 and H_∞ Control Problems," *Institute of Electrical and Electronic Engineers Transactions on Automatic Control*, Vol. AC-34, 1989, pp. 831–847.

[24]Chiang, R. Y., and Safonov, M. G., *Robust-Control Toolbox*, Mathworks, South Natick, MA, 1988.

[25]Leo, D. J., and Inman, D. J., "Modeling and Control Simulations of a Slewing Frame Containing Active Members," *Smart Materials and Structures Journal*, Vol. 2, No. 2, 1993, pp. 82–95.